

Can a Long Nanoflare Storm Explain the Observed Emission Measure Distributions in Active Region Cores?

Fana M. Mulu-Moore¹, Amy R. Winebarger¹, and Harry P. Warren²

ABSTRACT

All theories that attempt to explain the heating of the high temperature plasma observed in the solar corona are based on short bursts of energy. The intensities and velocities measured in the cores of quiescent active regions, however, can be steady over many hours of observation. One heating scenario that has been proposed to reconcile such observations with impulsive heating models is the “long nanoflare storm,” where short duration heating events occur infrequently on many sub-resolutions strands; the emission of the strands is then averaged together to explain the observed steady structures. In this Letter, we examine the emission measure distribution predicted for such a long nanoflare storm by modeling an arcade of strands in an active region core. Comparisons of the computed emission measure distributions with recent observations indicate that the long nanoflare storm scenario implies greater than 5 times more 1 MK emission than is actually observed for all plausible combinations of loop lengths, heating rates, and abundances. We conjecture that if the plasma had “super coronal” abundances, the model may be able to match the observations at low temperatures.

Subject headings: Sun: corona

1. Introduction

Determining the mechanism that heats the solar upper atmosphere is one of the central goals in observing the solar corona. Coronal heating theories predict short bursts of energy (Klimchuk 2006); these energy releases are often called “nanoflares,” though they are not necessarily caused by small-scale magnetic reconnection events (i.e. Parker’s nanoflares; Parker 1988). One interpretation of this type of heating has been discussed in a series of papers by Cargill and Klimchuk (Cargill 1994; Cargill & Klimchuk 1997, 2004; Klimchuk et al. 2008; Klimchuk 2009). They describe nanoflare heating as a single short-lived heating event that occurs *infrequently* on an elemental strand in the corona; the density and temperature of the plasma associated with the strand then evolve without any additional heating events. (We adopt the definition of “strand” as a fundamental flux tube in the corona and “loop” as an observed coronal structure. A loop may be formed of a single strand,

¹NASA Marshall Space Flight Center, VP 62, Huntsville, AL 35812; fanamariam.mulumoore@nasa.gov

²Space Science Division, Naval Research Laboratory, Washington, DC 20375

which would imply the corona is being resolved, or many, sub-resolution strands.) The evolution and other properties of warm EUV loops have been shown to be consistent with the Cargill and Klimchuk nanoflare model (e.g., Warren et al. 2002; Winebarger et al. 2003; Warren et al. 2003). In these loops, the nanoflares occur within a narrow heating envelope (a so-called “short nanoflare storm,” Klimchuk 2009) on a few sub-resolution strands, then the strands, and apparent loop, evolve.

In the core of active regions, however, the average apex intensity (Warren et al. 2010), footpoint intensity (Antiochos et al. 2003), and Doppler and non-thermal velocities (Brooks & Warren 2009) are often found to be steady (with variations of $\pm 20\%$) over several hours of observation, prompting some to suggest that the heating in active region cores is effectively steady, i.e., heating events occur *frequently* on a single strand in the corona (Schrijver et al. 2004; Warren & Winebarger 2006, 2007; Lundquist et al. 2008; Winebarger et al. 2008, 2011). Klimchuk (2009) has instead suggested that these loops are heated by “long nanoflare storms”, i.e. the loops are bundles of many strands and each strand is heated at a different time. After a single heating event, the plasma along the strand is allowed to cool completely with no additional heating events on the strand. At any given time in a loop’s evolution, it is composed of strands in all the different stages of the heating and cooling cycle so the dynamic properties of the plasma are “averaged out” in the observed loop. For this heating scenario, the observed loops would have some of the same properties as a frequently heated loop, such as steady intensity and velocity.

The purpose of this Letter is to test whether the emission measure distribution predicted by the long nanoflare storm model is consistent with the observed emission measure distributions in active region cores. We first calculate the expected temperature and density evolution for nine representative strands with a range of lengths and heating rates typical to active region cores using a one-dimensional hydrodynamic simulation. We complete the simulations twice, once with a radiative loss function consistent with photospheric abundances and once with a radiative loss function consistent with coronal abundances. We then predict the expected emission measure distribution of the loop by assuming the loop is composed of a bundle of strands that are each in a slightly different stage of the temperature and plasma evolution (similar to Klimchuk 2006, 2009; Patsourakos & Klimchuk 2009). We characterize the “cool” ($6.0 \leq \text{Log } T \leq \text{Log } T_{peak}$) emission measure distribution of each loop by assuming it can be represented by $EM \sim T^\alpha$ and finding α .

For the photospheric radiative loss function, we find $1.6 < \alpha < 2.0$ for all simulated loops. For the coronal radiative loss function, we find $2.0 < \alpha < 2.3$ for all simulated loops. Finally, we sum the emission measure distributions for all loops to approximate a potential emission measure distribution of an active region core where many loops may be along the line-of-sight. We find the summed distributions have $\alpha = 1.8$ for photospheric abundances and $\alpha = 2.0$ for coronal abundances. We compare these results to two recent analyses of active region cores, which had $3.1 < \alpha < 3.4$. We find that the long nanoflare storm scenario predicts > 5 times more 1 MK emission than is actually observed in the core of these active regions. The long nanoflare storm also predicts more high temperature (> 6 MK) emission than observed, but the observations are

not well constrained at those temperatures (Winebarger et al. 2011). Through this research, we have determined that the expected index, α , is sensitive to the abundances in the active region cores, with coronal abundances predicting larger values of α than photospheric abundances. We hypothesize that if the abundances in the active region core were “super-coronal” the long nanoflare storm simulation could reproduce the observed emission measure distribution.

2. Long Nanoflare Storm Model

In this section, we discuss the one-dimensional hydrodynamic simulations of nine representative strands. We consider three half-lengths (excluding the model chromosphere) of 25 Mm, 50 Mm and 100 Mm. We assume the strands are semi-circular, perpendicular to the solar surface, and symmetric (only the half loop solution is solved). We parameterize the spatial and temporal dependence of the energy deposition as

$$E_H(s, t) = E_0 + g(t)E_F \exp\left(\frac{(s - s_0)^2}{2\sigma_s^2}\right). \quad (1)$$

where s_0 designates the location of the peak of the heating function, σ_s is the spatial width of the heating function, and E_F determines the maximum amplitude of the heating function. Because symmetry is assumed, there will be two heating locations, one along each loop leg. The function $g(t)$ is chosen to be a simple triangular pulse,

$$g(t) = \begin{cases} t/\delta & 0 < t \leq \delta \\ (2\delta - t)/\delta & \delta < t \leq 2\delta, \end{cases} \quad (2)$$

where 2δ is the duration of the impulsive heating. The uniform background heating, E_0 , consistent with ~ 0.5 MK, is always applied, so the density and temperature will eventually return to a steady-state equilibrium.

In our simulations, the duration ($2\delta = 100$ s), width ($\sigma_s = 0.6$ Mm), and heating location ($s_0 = 0.5L$ where L is the half-length) of the impulsive heating function is the same for each simulation. We vary the magnitude of the heating, E_F , to achieve a specific equilibrium temperature (see Winebarger & Warren 2004) of 4, 5, or 6 MK based on the photospheric radiative loss function. The equilibrium temperature in an impulsive heating solution is the temperature at which the density, temperature, and loop length all agree with steady-state conditions. It is approximately the temperature at which the cooling switches from being dominated by conduction to being dominated by radiation. This is also approximately when the density of the solution peaks. The values of E_F are given in Column 3 of Table 1. These same heating magnitudes are applied to the simulations using coronal abundances.

For each of the lengths, equilibrium temperatures, and radiative loss functions (18 individual simulations), we solve the hydrodynamic loop equations with the Naval Research Laboratory Solar Flux Tube Model (NRL_SOLFTM). We adopt many of the same assumptions that were used in

previous simulations with this code, and we refer the reader to earlier papers for additional details of this numerical code (Mariska 1987; Mariska et al. 1989). The radiative loss functions used in the simulations are based on the atomic physics calculations with ionization equilibrium described by Mazzotta et al. (1998) and the abundances of Grevesse & Sauval (1998) for photospheric abundances and Feldman et al. (1992) for coronal abundances.

We compute average temperature and density evolution by averaging over the top 50% of the coronal part of the strand where $T_e > 2 \times 10^4$ K. As an example, the evolution of the 25 Mm half-length strand with a heating magnitude, E_F , of $7.5 \text{ erg cm}^{-3} \text{ s}^{-1}$ is shown in Figure 1. This example has an equilibrium temperature of 4 MK. The left panel shows the average temperature as a function of time and the right panel shows the average density as a function of time for both photospheric and coronal abundances. As the nanoflare is turned on, the average temperature rises rapidly. Similarly, the density begins to increase as chromospheric material fills the strand. As the heating event ends, first the temperature and then the density begin to decrease. The peak density is higher and the cooling time longer for the photospheric solution compared to the coronal solution.

Above we have described how the temperature and density evolution of representative strands were calculated. Here we discuss the method to combine these strands to determine properties of both individual loops and an active region core. First we assume that a loop is formed of many strands, with a single strand in each stage of the temperature and density evolution, similar to Klimchuk et al. (2008); Patsourakos & Klimchuk (2009). In practical terms, this assumption implies a loop contains one strand for each time step of the simulation. For instance, in the photospheric solution shown in Figure 1, the strand evolves for 2100 s before returning to equilibrium conditions. The code writes the solution every 10 s. The consequent loop, then, is formed of 210 strands, with each strand having an average temperature and density associated with a specific time step of the simulation.

The emission measure distribution of the loop is then determined by sorting the emission measures of the contributing strands into temperature bins. The emission measure for each strand is calculated from $n_e^2 ds$ where n_e is the average electron density of the strand and ds is the depth of the strand; this emission measure is placed in the bin containing the average temperature of the strand at that time step. The resulting emission measure distributions for each loop length, equilibrium temperature, and radiative loss assumptions are shown in Figure 2. The dotted vertical lines in Figure 2 mark the temperatures corresponding to the peak of the emission measure distributions; these peak temperatures are listed in Table 1. For each length and equilibrium temperature, the photospheric solutions are shown in blue and the coronal solutions are shown in red. We scale the emission measure distributions so that the peak in the EM curve is 10^{28} cm^{-5} .

From $\text{Log } T = 6.0$ to the temperature of the peak of the emission measure distribution, the emission measure distribution can be approximated as $EM \sim T^\alpha$. We determine α by fitting the log of the emission measure distribution as a function of log of temperature with a linear regression

routine. These fits are shown in Figure 2 and the values of α are given in Table 1. For photospheric abundances, α ranges from 1.6 to 2.0 and for coronal abundances α range from 2.0 to 2.3. In general, longer, hotter strands have larger α s. The coronal solutions have larger values of α than the photospheric solutions.

In the core of an active region, many loops are along the line-of-sight. To approximate the emission measure distribution for an active region core, we simply sum the emission measure distributions for either the photospheric or coronal abundances for all loops shown in Figure 2; these emission measure distributions are shown in Figure 3. We have normalized the emission measure distributions to $1 \times 10^{28} \text{ cm}^{-5}$ for ease of comparison. We also compute the α for the summed solutions and we find $\alpha = 1.8$ for photospheric abundances and $\alpha = 2.0$ for coronal abundances. These α represent an emission measure weighted average α of the individual loops. This implies that when an active region core is formed of many loops, the emission measure distribution of the core can never have an α smaller or larger than the minimum and maximum α for each constituent loop. For comparison, we show two emission measure distributions from observations; we discuss these in detail in the following section.

3. Discussion

In this Letter, we have investigated the emission measure distribution predicted by the long nanoflare storm heating scenario. We calculated an array of one-dimensional hydrodynamic solutions for three different lengths, three different equilibrium temperatures, and two assumed radiative loss functions. Next we computed average temperature and density evolution (Figure 1) by averaging over the upper 50% of the strand. We assumed a loop is a bundle of evolving strands with each strand in a different stage of the density and temperature evolution and generated an emission measure distribution for each loop. We have calculated the power-law indices, α , of the emission measure distributions for the temperature range $6.0 < \text{Log } T < \text{Log } T_{peak}$ for the simulated loops. These measurements are listed Table 1.

To approximate an active region core, where many loops are along the line-of-sight, we summed the emission measure distributions that are shown in Figure 2. The resulting emission measure distributions are presented in Figure 3. The power law indices of the summed emission measure distributions are 1.8 and 2.0 for photospheric and coronal abundances, respectively. We compare the summed emission measure distributions, shown in Figure 3, to two recently published emission measure distributions of active region cores. The power law indices of the observed emission measure distributions are ~ 3.2 (Warren et al. 2011; Winebarger et al. 2011). When comparing these values with the observations, we find that the long nanoflare storm predicts > 5 times more 1 MK emission than observed. We also note that the long nanoflare storm also predicts more high temperature (> 6 MK) emission than observed (see Figure 3), but we do not stress this result for several reasons. First, the observations are not well constrained at high temperatures (Winebarger et al. 2011). Also the high-temperature evolution of the hydrodynamic simulations, which occurs early

in the simulation when conduction dominates the energy equation, are greatly influenced by the location and duration of the heating event (see Winebarger & Warren (2004)). Finally, during this early stage, the plasma may be out of nonequilibrium ionization which would change the calculated emission measure distribution (see Bradshaw & Klimchuk (2011)).

One method of testing to see if the long nanoflare storm is viable is to examine line ratios observed in active region cores. Table 2 gives the expected EIS intensities for a few key EIS spectral lines for the summed coronal emission measure distribution shown in Figure 3. The last column of Table 2 is the ratio of the expected intensities to the expected intensity in the Ca XIV 193.874 Å line. For instance the expected ratio between the Fe XII 195.119 Å and the Ca XIV 193.874 Å lines is 13.56. Warren et al. (2011) determine the observed ratio is closer to 4.7. Also, the ratio between the Fe X 184.536 Å and Ca XIV 193.874 Å and Fe XV 284.160 Å and Ca XIV 193.874 Å are predicted to be ~ 3.6 and ~ 86.69 respectively; the observed ratios of these lines were ~ 0.9 and ~ 33.1 respectively in Warren et al. (2011).

We have presented emission measure distributions obtained from one-dimensional hydrodynamic simulations that combine plausible combinations of loops lengths, heating rates, and abundances similar to what is expected to be observed in the core of active regions. In early 0D nanoflare simulations, Cargill (1994) found the slope of the emission measure curve calculated from 10^6 K to the peak of the emission measure to be $3.5 < \alpha < 4.8$, though these results are based on simple assumptions of the cooling and draining of the plasma.

The one-dimensional hydrodynamic code used in this study can not currently deal with increasing cross sectional area of loops and cannot be used to assess how the expansion affects the solutions. The slope of the DEMs of loops with expanding cross sections has been shown to get steeper with increasing expansion factor (for example, see van den Oord et al. 1997) and we are working with a new code that would be able to examine the cross sectional area in the future.

The author, FMM, is supported by an appointment to NASA’s Postdoctoral Program (NPP) which is administered by Oak Ridge Associated Universities (ORAU). The authors would like to thank the NPP host facility, Marshall Space Flight Center, and are also grateful to the referee for providing helpful comments to improve the manuscript.

REFERENCES

- Antiochos, S. K., Karpen, J. T., DeLuca, E. E., Golub, L., & Hamilton, P. 2003, *ApJ*, 590, 547
- Bradshaw, S. J., & Klimchuk, J. A. 2011, *ApJS*, 194, 26
- Brooks, D. H., & Warren, H. P. 2009, *ApJ*, 703, L10
- Cargill, P. J. 1994, *ApJ*, 422, 381

- Cargill, P. J., & Klimchuk, J. A. 1997, *ApJ*, 478, 799
- Cargill, P. J., & Klimchuk, J. A. 2004, *ApJ*, 605, 911
- Feldman, U., Mandelbaum, P., Seely, J. F., Doschek, G. A., & Gursky, H. 1992, *ApJS*, 81, 387
- Grevesse, N., & Sauval, A. J. 1998, *Space Sci. Rev.*, 85, 161
- Klimchuk, J. A. 2006, *Sol. Phys.*, 234, 41
- Klimchuk, J. A. 2009, in *Astronomical Society of the Pacific Conference Series*, Vol. 415, *Astronomical Society of the Pacific Conference Series*, ed. B. Lites, M. Cheung, T. Magara, J. Mariska, & K. Reeves, 221
- Klimchuk, J. A., Patsourakos, S., & Cargill, P. J. 2008, *ApJ*, 682, 1351
- Lundquist, L. L., Fisher, G. H., & McTiernan, J. M. 2008, *ApJS*, 179, 509
- Mariska, J. T. 1987, *ApJ*, 319, 465
- Mariska, J. T., Emslie, A. G., & Li, P. 1989, *ApJ*, 341, 1067
- Mazzotta, P., Mazzitelli, G., Colafrancesco, S., & Vittorio, N. 1998, *A&AS*, 133, 403
- Parker, E. N. 1988, *ApJ*, 330, 474
- Patsourakos, S., & Klimchuk, J. A. 2009, *ApJ*, 696, 760
- Schrijver, C. J., Sandman, A. W., Aschwanden, M. J., & DeRosa, M. L. 2004, *ApJ*, 615, 512
- van den Oord, G. H. J., Schrijver, C. J., Camphens, M., Mewe, R., & Kaastra, J. S. 1997, *A&A*, 326, 1090
- Warren, H. P., Brooks, D., & Winebarger, A. R. 2011, *ApJ*, 734,90
- Warren, H. P., & Winebarger, A. R. 2006, *ApJ*, 645, 711
- Warren, H. P., & Winebarger, A. R. 2007, *ApJ*, 666, 1245
- Warren, H. P., Winebarger, A. R., & Brooks, D. H. 2010, *ApJ*, 711, 228
- Warren, H. P., Winebarger, A. R., & Hamilton, P. S. 2002, *ApJ*, 579, L41
- Warren, H. P., Winebarger, A. R., & Mariska, J. T. 2003, *ApJ*, 593, 1174
- Winebarger, A. R., Schmelz, J. T., Warren, H. P., Saar, S. H., & Kashyap, V. L. 2011, *ApJ*, accepted
- Winebarger, A. R., & Warren, H. P. 2004, *ApJ*, 610, L129

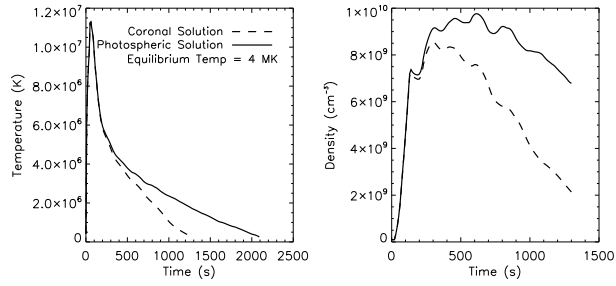


Fig. 1.— The evolution of an impulsively heated, 25 Mm half-length strand is shown. The average apex temperature (left) and density (right) are shown as a function of time for both photospheric (solid) and coronal (dashed) radiative loss functions.

Winebarger, A. R., Warren, H. P., & Falconer, D. A. 2008, *ApJ*, 676, 672

Winebarger, A. R., Warren, H. P., & Schmelz, J. T. e. a. 2011, *ApJ*, accepted

Winebarger, A. R., Warren, H. P., & Seaton, D. B. 2003, *ApJ*, 593, 1164

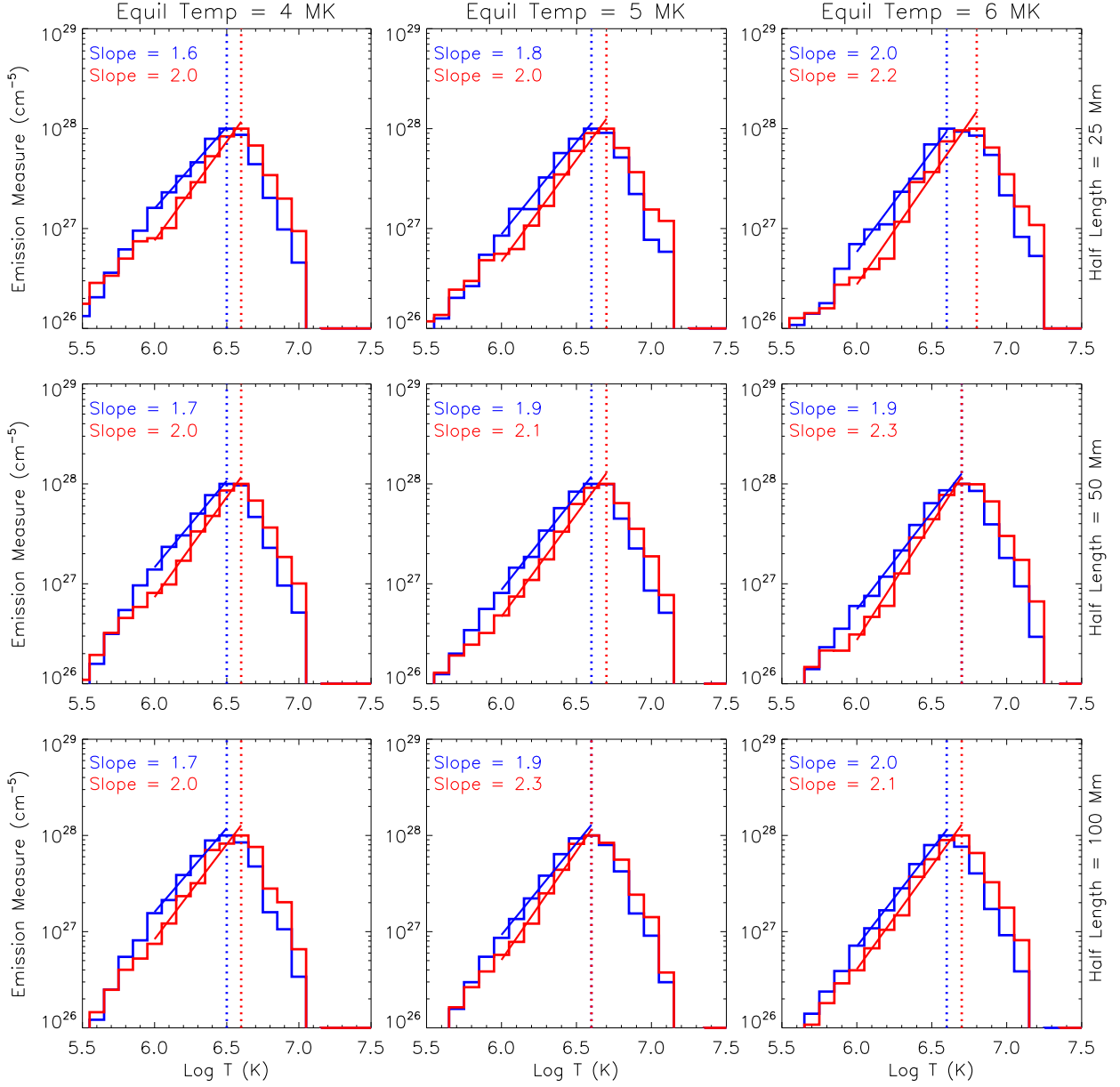


Fig. 2.— The first, second and third rows show the emission measure distributions of 25, 50 and 100 Mm half-length loops respectively. The first, second, and third columns show solutions with equilibrium temperatures of 4, 5, and 6 MK, respectively. In each plot, the photospheric solution is shown as a blue line and the coronal solution is shown as a red line. The fit of the emission measure distributions are shown as well. The vertical dotted lines mark the temperatures corresponding to the peak of the emission measure distributions.

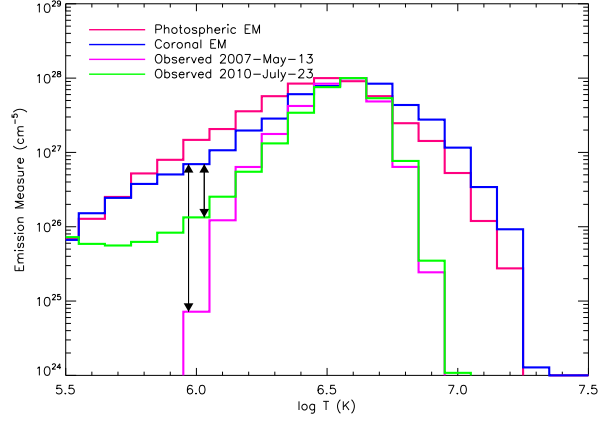


Fig. 3.— The average emission measure distribution from the different loops shown in Figure 2. For comparison, two emission measure distributions from two recent analyses are also shown Warren et al. (2011); Winebarger et al. (2011). We have normalized all the emission measure distributions to $1 \times 10^{28} \text{ cm}^{-5}$.

Table 1. Simulation Results

Half Length (Mm)	Equilibrium Temperature (MK)	Volumetric Heating Rate, E_F (ergs $\text{cm}^{-3} \text{ s}^{-1}$)	T_{PeakP} (MK)	α_P	T_{PeakC} (MK)	α_C
25	4	7.5	3.2	1.6	4.0	2.0
25	5	16.1	4.0	1.8	5.0	2.0
25	6	29.5	4.0	2.0	6.3	2.2
50	4	7.2	3.2	1.7	4.0	2.0
50	5	14.5	4.0	1.9	5.0	2.1
50	6	27.1	5.0	1.9	5.0	2.3
100	4	3.3	3.2	1.7	4.0	2.0
100	5	5.2	4.0	1.9	4.0	2.3
100	6	8.3	4.0	2.0	5.0	2.1
SUM			3.2	1.7	4.0	2.0

Table 2. Expected EIS intensities

EIS Spectral Line	Log T_{max}	I (ergs cm ⁻² s ⁻¹ sr ⁻¹)	I/I_{CaXIV}
Fe X 184.536Å	6.0	1076.9	3.62
Fe XI 180.401Å	6.1	3752.2	12.63
Fe XI 188.216Å	6.1	1912.2	6.43
Fe XII 192.394Å	6.1	1294.2	4.35
Fe XII 195.119Å	6.1	4031.3	13.56
S X 264.233Å	6.1	227.2	0.76
Si X 258.375Å	6.1	1133.9	3.82
Fe XIII 202.044Å	6.2	1425.0	4.80
Fe XIII 203.826Å	6.2	3930.6	13.23
Fe XIV 270.519Å	6.3	1482.4	4.99
Fe XIV 264.787Å	6.3	3246.6	10.92
Fe XV 284.160Å	6.3	25762.0	86.69
Fe XVI 262.984Å	6.4	1764.9	5.94
S XIII 256.686Å	6.4	1684.2	5.67
Ca XIV 193.874Å	6.5	297.2	1.00
Ca XV 200.972Å	6.6	223.6	0.75
Ca XVI 208.604Å	6.7	191.9	0.65
Ca XVII 192.858Å	6.7	424.5	1.43